

The most beautiful strongly bound dibaryon

Nilmani Mathur,^{1,*} M. Padmanath,^{2,†} and Debsubhra Chakraborty^{1,‡}

¹*Department of Theoretical Physics, Tata Institute of Fundamental Research, Homi Bhabha Road, Mumbai 400005, India.*

²*Helmholtz Institut Mainz, Staudingerweg 18, 55128 Mainz, Germany
GSI Helmholtzzentrum für Schwerionenforschung, Darmstadt, Germany*

We report the first lattice quantum chromodynamics (QCD) study of the heavy dibaryons in which all six quarks have the bottom (beauty) flavor. Performing a state-of-the-art lattice QCD calculation, with full control over relevant systematic errors, we find clear evidence for a deeply bound Ω_{bbb} - Ω_{bbb} dibaryon in the 1S_0 channel, as a pole singularity in the S -wave Ω_{bbb} - Ω_{bbb} scattering amplitude with a binding energy $-89(^{+16}_{-12})$ MeV. With such a deep binding, Coulomb repulsion serves only as a perturbation on the ground state wave-function of the parameterized strong potential and may shift the strong binding only by a few percent. Considering the scalar channel to be the most bound for single flavored dibaryons, we conclude this state is the heaviest possible most deeply-bound dibaryon in the visible universe.

PACS numbers: 12.38.Gc, 12.38.-t, 14.20.Lq

Understanding baryon-baryon interactions from first principles is of prime interest in nuclear physics, cosmology and astrophysics. They form a fundamental ingredient in big-bang nucleosynthesis, in the formation of atomic nuclei and their structures, nuclear fusion in stars, and in dense matter [1–4]. Dibaryons are the simplest nuclei with baryon number 2, in which such interactions can be studied transparently. However, the only known stable dibaryon is deuteron, and just one more unstable light dibaryon ($d^*(2380)$) has recently been observed [5]. Even so, based on the theory of strong interactions, one expects to have more dibaryons in Nature, particularly with the strange and heavy quark contents. *Ab-initio* theoretical investigations using lattice QCD are well suited for studying such hadrons and indeed can play a major role in their future discovery.

Although lattice QCD calculations of dibaryon systems are becoming more feasible now [6–10], such studies on heavy dibaryons are limited to only two calculations [11, 12]. Among the heavy dibaryons, a system of two Ω_{QQQ} baryons ($Q \equiv c, b$) is of prime interest as they provide unique opportunity to investigate baryon-baryon interactions and associated non-perturbative features of QCD in a chiral dynamics free environment. Lattice QCD investigation of Ω_{ccc} - Ω_{ccc} dibaryon reported a shallow bound state in the 1S_0 channel [12]. On the other hand, lattice studies on the deuteron-like dibaryons [11] and tetraquarks [13–16] have shown that multi-hadrons with multiple bottom quarks can have deep bindings. It is thus very timely to study Ω_{bbb} - Ω_{bbb} interactions using lattice QCD given that very little is known about it through phenomenological models [17–19]. Such studies not only can stimulate search for heavy dibaryons, they can also provide theoretical understanding of the strong dynamics of heavy quarks and quark-mass dependence of scattering parameters.

In this letter, we report the first lattice QCD inves-

tigation of the ground state of the dibaryons with the highest number of bottom (beauty) quarks in the 1S_0 channel. We name it $\mathcal{D}_{6b} \equiv \Omega_{bbb}$ - Ω_{bbb} , a dibaryon formed out of a combination of two Ω_{bbb} baryons. Utilizing various state-of-the-art lattice QCD utilities and methodologies, we extract the mass of \mathcal{D}_{6b} and find clear evidence for a strongly bound state, with a binding energy of $-89(^{+16}_{-12})(12)$ MeV, and a scattering length of $0.17(^{+0.01}_{-0.02})(0.02)$ fm. Despite its compactness, we find the Coulomb interactions act only as a perturbation to the strong interactions and do not change the binding in any significant way. Upon comparison to the binding energies of other dibaryons, *e.g.* 2.2 MeV of deuteron, and other strange/heavy dibaryons [11, 12], we conclude \mathcal{D}_{6b} to be the most deeply bound heaviest possible dibaryon in our visible universe.

The lattice set up that we utilize here is similar to that were used in Refs. [15, 20] and we discuss it below.

A. Lattice ensembles: We employ four lattice QCD ensembles with dynamical u/d , s and c quark fields, generated by MILC collaboration [21] with HISQ fermion action [22], as shown in Figure 1. Lattice spacings are determined using r_1 parameter [21], which are found to be consistent with the scales obtained through Wilson-flow [23].

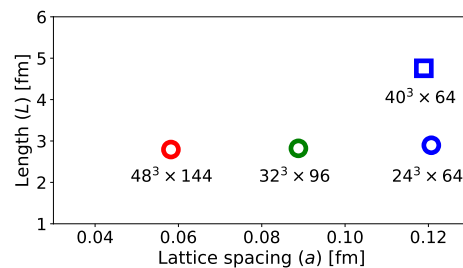


FIG. 1. Lattice QCD ensembles, with sizes $N_s^3 \times N_t$, used in this work. Here $L = N_s a$ is the spatial extent of the lattice.

B. Bottom quarks on lattice: Since the bottom quark is very heavy, we use a non-relativistic QCD (NRQCD) Hamiltonian [24], including improvement coefficients up to $\mathcal{O}(\alpha_s v^4)$ [25]. Quark propagators are calculated from the evolution of NRQCD Hamiltonian with Coulomb gauge fixed wall sources at multiple source time-slices. We tune the bottom quark mass using the Fermilab prescription for heavy quarks [26] in which we equate the lattice-extracted spin-averaged kinetic mass of the 1S bottomonia states with its physical value [27]. Such a tuning was also utilized in Refs. [11, 15, 20] and was found to reproduce the physical value of the hyperfine splitting of 1S bottomonia.

C. (Di)baryon interpolators: For the single Ω_{bbb} baryon, we utilize the quasi-local non-relativistic operator with $J^P = 3/2^+$, as was used by LHPC-collaboration and are listed in Table VII of Ref. [28]. For extracting the ground state mass we assume only S -wave interactions in two baryon systems where the overall state is anti-symmetric under the exchange of two baryons. Denoting components of the $J=3/2$ Ω_{bbb} operator ($\mathcal{O}_{\Omega_{bbb}}$) with χ_m , m being the azimuthal component of J , we construct the Ω_{bbb} - Ω_{bbb} dibaryon operators as,

$$\mathcal{O}_{\mathcal{D}_{6b}}(x, t) = \chi_m [CG]^{mn} \chi_n. \quad (1)$$

Here $[CG]^{mn}$ are the relevant spin-projection matrix constructed out of the appropriate Clebsh-Gordon coefficients. For example, the $J = 0$ operator is given by,

$$\mathcal{O}_{\mathcal{D}_{6b}^{J=0}} = \frac{1}{2} \left[\chi_{\frac{3}{2}} \chi_{-\frac{3}{2}} + \chi_{-\frac{1}{2}} \chi_{\frac{1}{2}} - \chi_{\frac{1}{2}} \chi_{-\frac{1}{2}} - \chi_{-\frac{3}{2}} \chi_{\frac{3}{2}} \right]. \quad (2)$$

Using these baryon and dibaryon operators ($\mathcal{O}_{\Omega_{bbb}}$ and $\mathcal{O}_{\mathcal{D}_{6b}}$) we compute two-point correlation functions between the source (t_i) and sink (t_f) time-slices,

$$C_{\mathcal{O}}(t_i, t_f) = \sum_{\vec{x}} e^{-i\vec{p}\cdot\vec{x}} \langle 0 | \mathcal{O}(\vec{x}_f, t_f) \bar{\mathcal{O}}(\vec{x}_i, t_i) | 0 \rangle. \quad (3)$$

Ground state mass in each channels is obtained by fitting the respective average correlation function with a single exponential at sufficiently large times ($\tau = t_f - t_i$).

While determining mass in a lattice calculation it is often useful to plot the effective mass, defined as $m_{eff}a = \log[\langle C(\tau) \rangle / \langle C(\tau+1) \rangle]$, to show the signal saturation and justify the time-window to be chosen in the exponential fit. In Figure 2, we present the effective masses for $C_{\Omega_{bbb}}^2$ (green circles) and $C_{\mathcal{D}_{6b}}$ (blue squares) on the finest ensemble ($a \sim 0.06$ fm). We make the following observations from this result: (I) The signal in the effective masses saturates well before the noise takes over, and hence one can reliably extract the respective ground state masses. (II) The signal in the noninteracting $2\Omega_{bbb}$ level survives until large times. This is because $2\Omega_{bbb}$ level is obtained from the single baryon Ω_{bbb} correlator which decays with an exponent of $M_{\Omega_{bbb}} < M_{\mathcal{D}_{6b}}$, and hence can

propagate further than the \mathcal{D}_{6b} state. (III) Most importantly, it is quite evident that there is a clear energy-gap between the ground state energy levels of the noninteracting two-baryon and the dibaryon systems at all times. This clearly shows that the ground state mass of dibaryon $M_{\mathcal{D}_{6b}}$ is smaller than that of the non-interacting level $2M_{\Omega_{bbb}}$. We find similar energy differences for all the ensembles and we discuss the results below.

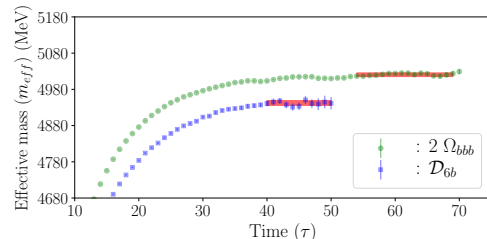


FIG. 2. Effective masses corresponding to the ground states of the non-interacting two-baryon and dibaryon correlators on the finest lattice ensemble. An energy gap between them is clearly visible at all time slices. The solid bands show the fit-estimates and fit-windows.

In Figure 3 we show the fitted results for two ensembles at two different lattice volumes – the left column is for the energy of the Ω_{bbb} level while the right column represents the mass of the dibaryon \mathcal{D}_{6b} . The data-points in the figure present the dependence of the initial time (τ_{min}) considered in the exponential fit for a given final time (τ_{max}), just before the signal is lost in the statistical noise. In each subplot the red-line indicates the best fit value at the chosen τ_{min} , while the blue band show its 1σ band. We also add the systematic uncertainty arising out of various fit windows, and together with the statistical error, magenta bands show the total fit error. Statistical uncertainties are estimated using bootstrap method, considering the central 68% of the samples. Results for other two lattices are shown in the supplemental material [29].

Next we calculate the energy difference between the ground state of the dibaryon (\mathcal{D}_{6b}) and the non-interacting two-baryons ($2\Omega_{bbb}$)

$$\Delta E = M_{\mathcal{D}_{6b}} - 2M_{\Omega_{bbb}}. \quad (4)$$

In Table I, we present ΔE for all the lattice ensembles and find it to be always *negative* and several standard deviations (σ) away from zero. This observation on multiple ensembles, with three different lattice spacings and two different volumes, lead us to unambiguously conclude that there is an energy level below the threshold.

Scattering analysis: To establish the existence of a state from these energy levels in terms of pole singularities in the $\Omega_{bbb}\Omega_{bbb}$ S -wave scattering amplitudes across the complex Mandelstam s -plane, we utilize the generalized form of finite-volume formalism proposed by M. Lüscher

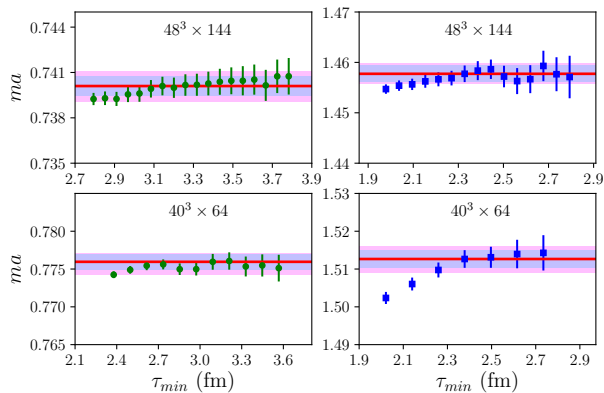


FIG. 3. Fit results for the ground state masses of Ω_{bbb} (left-column) and \mathcal{D}_{bb} (right-column) for various fit-windows with different choices of minimum time (τ_{min}) for two different lattice ensembles. The red lines are the chosen fits with blue bands as 1σ -band. The uncertainty in the choice of τ_{min} is incorporated by the magenta bands.

Ensemble	ΔE	Ensemble	ΔE
$24^3 \times 64$	$-64(11)$	$40^3 \times 64$	$-65(7)$
$32^3 \times 96$	$-72(9)$	$48^3 \times 144$	$-75(7)$

TABLE I. Energy difference $\Delta E = M_{\mathcal{D}_{bb}} - 2M_{\Omega_{bbb}}$ in MeV on different ensembles.

[30]. For the scattering of two spin-3/2 particles in the S -wave leading to a total angular momentum and parity $J^P = 0^+$, the phase shifts $\delta_0(k)$ are related to the finite-volume energy spectrum via Lüscher's relation

$$k \cot(\delta_0(k)) = \frac{2Z_{00}(1; (\frac{kL}{2\pi})^2)}{L\sqrt{\pi}}. \quad (5)$$

Here, k is the momentum of Ω_{bbb} in the centre of momentum frame and is given by

$$k^2 = \frac{\Delta E}{4}(\Delta E + 4M_{\Omega_{bbb}}^{phys}), \quad (6)$$

where ΔE is the energy differences listed in Table I, and $M_{\Omega_{bbb}}^{phys}$ is the mass of Ω_{bbb} in the continuum limit. The S -wave scattering amplitude is given by $t = (\cot\delta_0 - i)^{-1}$, and a pole in t related to a bound state happens when $k \cot\delta_0 = -\sqrt{-k^2}$. We parameterize $k \cot\delta_0 = -1/a_0$, where a_0 is the scattering length. The scattering analysis is performed following the procedure outlined in Appendix B of Ref. [31], such that the best fit parameters are constrained to satisfy Eq. (5). To estimate the systematic uncertainties from the lattice cut-off effects, we perform several different fits involving different subsets of the four levels with $k \cot\delta_0$ parameterized either as a constant or as a constant plus a linear term in the lattice spacing. All of the fits indicate the existence of a deeply bound state. We find that the best

fit corresponds to the one that considers all energy levels and incorporates the lattice spacing a dependence of the scattering length with a linear parameterization $k \cot\delta_0 = -1/a_0^{[0]} - a/a_0^{[1]}$. We present this as our main result, leading to a $\chi^2/d.o.f = 0.8/2$, with the following best fit parameters and binding energy

$$a_0^{[0]} = 0.17_{(-0.02)}^{(+0.01)} \text{ fm}, \quad a_0^{[1]} = -0.14_{(-0.06)}^{(+0.18)} \text{ fm}^2, \quad (7)$$

$$\text{and } \Delta E_{\mathcal{D}_{bb}} = -89_{(-12)}^{(+16)} \text{ MeV}. \quad (8)$$

In Figure 4, we present details of our main results. On the top pane, the analytically reconstructed finite-volume energy levels (black stars) from best fit parameters in Eq. (7) can be seen to be in agreement the simulated energy levels (large symbols), indicating quality of fit. In the middle pane, we plot $k \cot\delta_0$ versus k^2 in units of the energy of the threshold. The orange dashed curve is the bound state constraint $\sqrt{-k^2}$ and the red solid line is the fitted $k \cot\delta_0$ in the continuum limit. The crossing between these two curves, highlighted by the magenta symbol, is the bound state pole position in t . In the bottom pane, we present the continuum extrapolation of binding energy leading to the value in Eq. (8) compared with the simulated energy levels at the respective lattice spacings.

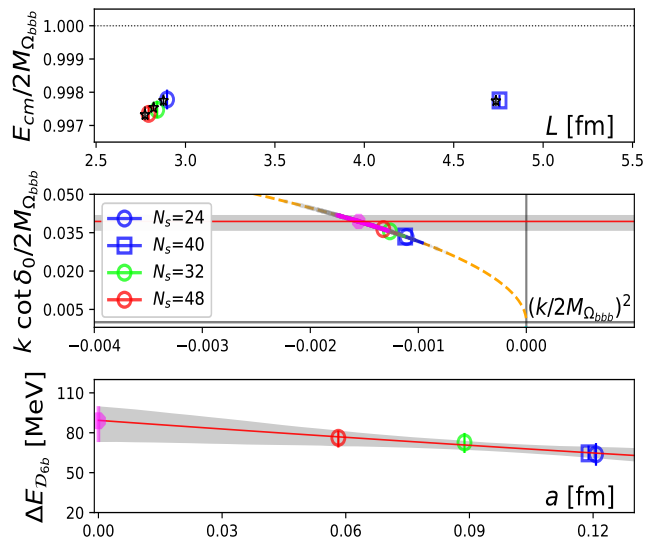


FIG. 4. Top: Comparison of the simulated energy levels (large symbols) with the energy levels (black stars) analytically reconstructed using Eq. (7), indicating the quality of the scattering analysis fit. Middle: $k \cot\delta_0$ versus k^2 in units of energy of the threshold ($2M_{\Omega_{bbb}}$) and information on poles in t indicated by magenta symbols. Bottom: Continuum extrapolation of the binding energy in Eq. (8) determined from fitted scattering amplitude in Eq. (7). Further details can be found in the discussion on scattering analysis.

Coulomb repulsion: With two units of electric charge in the system, the effect of Coulomb repulsion on the

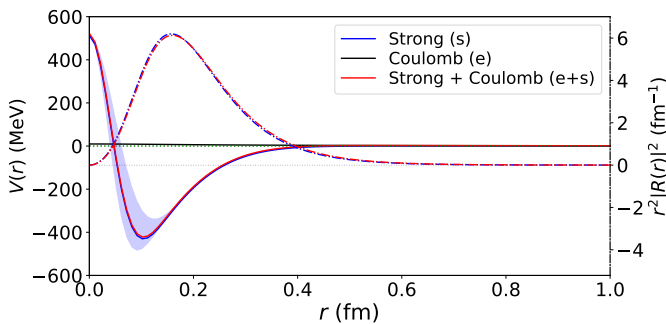


FIG. 5. Coulomb (V_e), the parameterized strong potentials (V_s) and their sum are shown by the black, blue and red curves, respectively. The shaded region represents the variation of V_s with respect to its parameters. V_e is evaluated at a *rms* charge radius equal to the *rms* radius of the V_s ground state. The radial probability densities of the ground state wave-functions of the strong and combined potentials are shown by the dashed-dotted curves.

binding energy of this dibaryon could be important. To gauge that, we perform the following analysis as in Ref. [12]. First, we model the strong interactions between two interacting Ω_{bbb}^- baryons with a quantum mechanical multi-Gaussian attractive potential V_s [12], constrained to match the binding energy $-89^{(+16)}_{(-12)}$ MeV that we find in this work. Next, we assume the form of the Coulomb potential (V_e) of Ω_{bbb}^- to be similar to that of Ω_{ccc}^{++} , except the total electric charge is -2 . We present a comparison of the strengths of these potentials as a function of the radial distance in Figure 5, with the root-mean-square (*rms*) charge radius r_d chosen as the *rms* radius of the ground state of V_s . Next, we solve the energy eigenvalue problem with the effective potential ($V_{eff} = V_s + V_e$) and determine the scattering length a_0^{e+s} and effective range r^{e+s} , following the procedure discussed in Ref. [12]. The radial probability densities of the ground state wave-functions (dashed-dotted curves) corresponding to V_s and V_{eff} are shown in Figure 5. It is evident that the Coulomb repulsion serves only as a perturbation and hence does not change the binding energy of \mathcal{D}_{6b} in any significant way. We also vary r_d and find that the effect of Coulomb repulsion is largely perturbative and binding may reduce at most by 10 MeV even when r_d is chosen to be unphysically low as 0.01 fm. We present $1/a_0^{e+s}$ for V_{eff} as a function of the Coulomb interaction strength α^e in Figure 6. Note that $1/a_0^{e+s}$ remains to be very much *positive* even at $\alpha^e = \alpha_{phys}^e$, confirming that \mathcal{D}_{6b} remains to be a deeply bound state even in the presence of Coulomb repulsion, with a total binding energy of about -85 MeV.

The final value of the dibaryon mass is determined by adding $\Delta E_{\mathcal{D}_{6b}}$ ($-89^{(+16)}_{(-12)}$) MeV with the two-baryon mass $2M_{\Omega_{bbb}}$. Since the Ω_{bbb} baryon mass is unknown we use its lattice extracted value. To this end, we perform continuum extrapolation of the energy

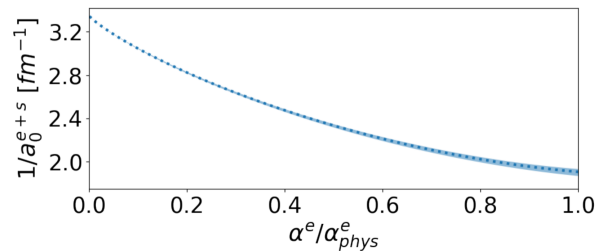


FIG. 6. The inverse of the scattering length $1/a_0^{e+s}$ as a function of α^e/α_{phys}^e . Its large *positive* value throughout indicates that \mathcal{D}_{6b} is a deeply bound state even in the presence of Coulomb repulsion.

splitting $M_{\Omega_{bbb}}(a) - \frac{3}{2}M_{\overline{1S}}(a)$, and then add $3/2M_{\overline{1S}}^{phys}$, with $M_{\overline{1S}}^{phys} = 9445$ MeV [32], to that. Thus we arrive at $M_{\Omega_{bbb}}^{phys} = 14366(7)(9)$ MeV, which is consistent with other lattice results [33]. Using that, we obtain $M_{\mathcal{D}_{6b}}^{phys} = 2M_{\Omega_{bbb}}^{phys} + \Delta E_{\mathcal{D}_{6b}} = 28643^{(+14)}_{(-17)}(15)$ MeV. Possible effects of Coulomb repulsion are included in the systematic errors.

Error budget: Finally we address the possible sources of errors in this calculation. We use a lattice set up with 2+1+1 flavored HISQ fermions where the gauge fields are Symanzik-improved at $\mathcal{O}(\alpha_s a^2)$, and the NRQCD Hamiltonian has improvement coefficients up to $\mathcal{O}(\alpha_s v^4)$. Such a lattice set up has shown to reproduce energy splittings in bottomonia with a uncertainty of about 6 MeV [29]. It is to be noted that here we are calculating the energy difference in which some of the systematics get reduced. For the dibaryon energy difference, statistical and fit-window errors are the main sources of error. The energy levels are extracted at sufficiently large times (~ 2.5 fm) and correlated averages with various fitting intervals are considered to arrive at conservative fitting-window errors. Statistical and fit window errors are added in quadrature, and then convolved through the Lüscher's analysis and continuum extrapolation, yielding a total error of about 18% for the binding energy. Other possible sources of errors are related to the continuum extrapolation fit forms, scale setting, quark mass tuning and electromagnetic corrections which together are found to be 12 MeV in such energy splittings, as detailed in the supplemental material [29].

Summary and Outlook: In this Letter, using lattice QCD we present a first investigation of the dibaryons in which all six quarks have bottom flavor and find a deeply bound dibaryon ($\mathcal{D}_{6b} \equiv \Omega_{bbb}-\Omega_{bbb}$) in the 1S_0 channel. Following Lüscher's formalism, we determine the relevant scattering amplitude, and after considering all possible systematic uncertainties, we identify a bound state pole with a binding energy $-89^{(+16)}_{(-12)}$ MeV relative to the threshold $2M_{\Omega_{bbb}}$. The mass of \mathcal{D}_{6b} dibaryon corresponding to this pole is found to be $28643^{(+14)}_{(-17)}(15)$ MeV. Although this dibaryon is expected to be compact, we find

the Coulomb repulsion within this dibaryon acts only as a perturbation to the strong interactions and may shift the mass only by a few percent.

It is interesting to observe that the bindings for similar dibaryons but at the strange and charm quark masses, \mathcal{D}_{6s} and \mathcal{D}_{6c} , were found to be about 1.6 and 5.7 MeV, respectively [12, 34]. Compared to those the binding energy of \mathcal{D}_{6b} is quite large. Deep bindings for heavy tetraquarks [13–16, 35, 36] and deuteron-like dibaryons with bottom quarks [11] have also been found. Perhaps the presence of more than one bottom quarks enhance the binding in multi-hadron systems which becomes maximum for \mathcal{D}_{6b} , making it to be the heaviest possible most deeply bound dibaryon in our visible universe. It would be interesting to investigate the quark mass dependence of scattering parameters and the onset of large binding by repeating this work over a wide range of quark masses systematically. Due to its heavy mass, it may not be possible to search \mathcal{D}_{6b} in the currently available experimental data. However, considering its unusually large binding it would be worthwhile to search this dibaryon in next generation experiments.

This work is supported by the Department of Atomic Energy, Government of India, under Project Identification Number RTI 4002. We are thankful to the MILC collaboration and in particular to S. Gottlieb for providing us with the HISQ lattice ensembles. We thank D. Mohler for a careful reading of the manuscript. We thank the authors of Ref. [37] for making the *TwoHadronsInBox* package utilized in this work and in particular Colin Morningstar for his help with the package. We also thank Takumi Doi and S. Paul for discussions. Computations are carried out on the Cray-XC30 of ILGTI, TIFR. N. M. would also like to thank A. Salve, K. Ghadiali and P. M. Kulkarni for computational supports.

* nilmani@theory.tifr.res.in

† pmadanag@uni-mainz.de

‡ debsubra@theory.tifr.res.in

- [1] R. V. Wagoner, W. A. Fowler, and F. Hoyle, On the Synthesis of Elements at Very High Temperatures, *Astrophys. J.* **148**, 3 (1967).
- [2] D. N. Schramm and M. S. Turner, Big-bang nucleosynthesis enters the precision era, *Rev. Mod. Phys.* **70**, 303 (1998).
- [3] E. Epelbaum, H.-W. Hammer, and U.-G. Meißner, Modern theory of nuclear forces, *Rev. Mod. Phys.* **81**, 1773 (2009).
- [4] C. Drischler, W. Haxton, K. McElvain, E. Mereghetti, A. Nicholson, P. Vranas, and A. Walker-Loud, Towards grounding nuclear physics in QCD, *Prog. Part. Nucl. Phys.* **121**, 103888 (2021), arXiv:1910.07961 [nucl-th].
- [5] A. P. et al. (WASA-at-COSY Collaboration and SAID Data Analysis Center), Evidence for a new resonance from polarized neutron-proton scattering, *Phys. Rev. Lett.* **112**, 202301 (2014).
- [6] S. R. Beane, E. Chang, W. Detmold, B. Joo, H. W. Lin, T. C. Luu, K. Orginos, A. Parreño, M. J. Savage, A. Torok, and A. Walker-Loud (NPLQCD Collaboration), Evidence for a bound h dibaryon from lattice qcd, *Phys. Rev. Lett.* **106**, 162001 (2011).
- [7] T. Inoue, N. Ishii, S. Aoki, T. Doi, T. Hatsuda, Y. Ikeda, K. Murano, H. Nemura, and K. Sasaki (HAL QCD), Bound H-dibaryon in Flavor SU(3) Limit of Lattice QCD, *Phys. Rev. Lett.* **106**, 162002 (2011), arXiv:1012.5928 [hep-lat].
- [8] Z.-H. Luo, M. Loan, and Y. Liu, Search for H dibaryon on the lattice, *Phys. Rev. D* **84**, 034502 (2011), arXiv:1106.1945 [hep-lat].
- [9] A. Francis, J. R. Green, P. M. Junnarkar, C. Miao, T. D. Rae, and H. Wittig, Lattice QCD study of the H dibaryon using hexaquark and two-baryon interpolators, *Phys. Rev. D* **99**, 074505 (2019), arXiv:1805.03966 [hep-lat].
- [10] J. R. Green, A. D. Hanlon, P. M. Junnarkar, and H. Wittig, Weakly Bound H Dibaryon from SU(3)-Flavor-Symmetric QCD, *Phys. Rev. Lett.* **127**, 242003 (2021), arXiv:2103.01054 [hep-lat].
- [11] P. Junnarkar and N. Mathur, Deuteronlike Heavy Dibaryons from Lattice Quantum Chromodynamics, *Phys. Rev. Lett.* **123**, 162003 (2019), arXiv:1906.06054 [hep-lat].
- [12] Y. Lyu, H. Tong, T. Sugiura, S. Aoki, T. Doi, T. Hatsuda, J. Meng, and T. Miyamoto, Dibaryon with Highest Charm Number near Unitarity from Lattice QCD, *Phys. Rev. Lett.* **127**, 072003 (2021), arXiv:2102.00181 [hep-lat].
- [13] P. Bicudo and M. Wagner (European Twisted Mass), Lattice QCD signal for a bottom-bottom tetraquark, *Phys. Rev. D* **87**, 114511 (2013), arXiv:1209.6274 [hep-ph].
- [14] A. Francis, R. J. Hudspith, R. Lewis, and K. Maltman, Lattice Prediction for Deeply Bound Doubly Heavy Tetraquarks, *Phys. Rev. Lett.* **118**, 142001 (2017), arXiv:1607.05214 [hep-lat].
- [15] P. Junnarkar, N. Mathur, and M. Padmanath, Study of doubly heavy tetraquarks in Lattice QCD, *Phys. Rev. D* **99**, 034507 (2019), arXiv:1810.12285 [hep-lat].
- [16] L. Leskovec, S. Meinel, M. Pflaumer, and M. Wagner, Lattice qcd investigation of a doubly-bottom $bbud$ tetraquark with quantum numbers $i(J^P) = 0(1^+)$, *Phys. Rev. D* **100**, 014503 (2019).
- [17] H. Huang, J. Ping, X. Zhu, and F. Wang, Full heavy dibaryons, (2020), arXiv:2011.00513 [hep-ph].
- [18] M.-Z. Liu and L.-S. Geng, Prediction of an Ω_{bbbb} Dibaryon in the Extended One-Boson Exchange Model, *Chin. Phys. Lett.* **38**, 101201 (2021), arXiv:2107.04957 [hep-ph].
- [19] J.-M. Richard, A. Valcarce, and J. Vijande, Very heavy flavored dibaryons, *Phys. Rev. Lett.* **124**, 212001 (2020), arXiv:2005.06894 [hep-ph].
- [20] N. Mathur, M. Padmanath, and S. Mondal, Precise predictions of charmed-bottom hadrons from lattice QCD, *Phys. Rev. Lett.* **121**, 202002 (2018), arXiv:1806.04151 [hep-lat].
- [21] A. Bazavov, C. Bernard, J. Komijani, C. DeTar, L. Levkova, W. Freeman, S. Gottlieb, R. Zhou, U. M. Heller, J. E. Hetrick, J. Laiho, J. Osborn, R. L. Sugar, D. Toussaint, and R. S. Van de Water (MILC Collabora-

- tion), Lattice qcd ensembles with four flavors of highly improved staggered quarks, *Phys. Rev. D* **87**, 054505 (2013).
- [22] E. Follana, Q. Mason, C. Davies, K. Hornbostel, G. P. Lepage, J. Shigemitsu, H. Trottier, and K. Wong (HPQCD, UKQCD), Highly improved staggered quarks on the lattice, with applications to charm physics, *Phys. Rev. D* **75**, 054502 (2007), arXiv:hep-lat/0610092 [hep-lat].
- [23] A. Bazavov, C. Bernard, N. Brown, J. Komijani, C. Detar, J. Foley, L. Levkova, S. Gottlieb, U. M. Heller, J. Laiho, R. L. Sugar, D. Toussaint, and R. S. Van de Water (MILC Collaboration), Gradient flow and scale setting on milc hisq ensembles, *Phys. Rev. D* **93**, 094510 (2016).
- [24] G. P. Lepage, L. Magnea, C. Nakhleh, U. Magnea, and K. Hornbostel, Improved nonrelativistic QCD for heavy quark physics, *Phys. Rev. D* **46**, 4052 (1992), arXiv:hep-lat/9205007 [hep-lat].
- [25] R. J. Dowdall, B. Colquhoun, J. O. Daldrop, C. T. H. Davies, I. D. Kendall, E. Follana, T. C. Hammant, R. R. Horgan, G. P. Lepage, C. J. Monahan, and E. H. Müller (HPQCD Collaboration), The upsilon spectrum and the determination of the lattice spacing from lattice qcd including charm quarks in the sea, *Phys. Rev. D* **85**, 054509 (2012).
- [26] A. X. El-Khadra, A. S. Kronfeld, and P. B. Mackenzie, Massive fermions in lattice gauge theory, *Phys. Rev. D* **55**, 3933 (1997), arXiv:hep-lat/9604004 [hep-lat].
- [27] M. Tanabashi *et al.* (Particle Data Group), Review of particle physics, *Phys. Rev. D* **98**, 030001 (2018).
- [28] S. Basak, R. Edwards, G. T. Fleming, U. M. Heller, C. Morningstar, D. Richards, I. Sato, and S. J. Wallace (Lattice Hadron Physics (LHPC)), Clebsch-Gordan construction of lattice interpolating fields for excited baryons, *Phys. Rev. D* **72**, 074501 (2005), arXiv:hep-lat/0508018.
- [29] *Results for other lattices, fit details and error budget are shown here.*
- [30] M. Luscher, Two particle states on a torus and their relation to the scattering matrix, *Nucl. Phys. B* **354**, 531 (1991).
- [31] M. Padmanath and S. Prelovsek, Evidence for a doubly charm tetraquark pole in DD^* scattering on the lattice, (2022), arXiv:2202.10110 [hep-lat].
- [32] P. Zyla *et al.* (Particle Data Group), Review of Particle Physics, *PTEP* **2020**, 083C01 (2020).
- [33] Z. S. Brown, W. Detmold, S. Meinel, and K. Orginos, Charmed bottom baryon spectroscopy from lattice QCD, *Phys. Rev. D* **90**, 094507 (2014), arXiv:1409.0497 [hep-lat].
- [34] S. Gongyo, K. Sasaki, S. Aoki, T. Doi, T. Hatsuda, Y. Ikeda, T. Inoue, T. Iritani, N. Ishii, T. Miyamoto, and H. Nemura (HAL QCD Collaboration), Most strange dibaryon from lattice qcd, *Phys. Rev. Lett.* **120**, 212001 (2018).
- [35] M. Karliner and J. L. Rosner, Discovery of doubly-charmed Ξ_{cc} baryon implies a stable $(bb\bar{u}\bar{d})$ tetraquark, *Phys. Rev. Lett.* **119**, 202001 (2017), arXiv:1707.07666 [hep-ph].
- [36] E. J. Eichten and C. Quigg, Heavy-quark symmetry implies stable heavy tetraquark mesons $Q_i Q_j \bar{q}_k \bar{q}_l$, *Phys. Rev. Lett.* **119**, 202002 (2017), arXiv:1707.09575 [hep-ph].
- [37] C. Morningstar, J. Bulava, B. Singha, R. Brett, J. Fallica, A. Hanlon, and B. Hörz, Estimating the two-particle K -matrix for multiple partial waves and decay channels from finite-volume energies, *Nucl. Phys. B* **924**, 477 (2017), arXiv:1707.05817 [hep-lat].
- [38] S. Beane, W. Detmold, K. Orginos, and M. Savage, Nuclear physics from lattice qcd, *Progress in Particle and Nuclear Physics* **66**, 1 (2011).
- [39] S. Borsanyi *et al.*, Ab initio calculation of the neutron-proton mass difference, *Science* **347**, 1452 (2015), arXiv:1406.4088 [hep-lat].
- [40] C. McNeile, C. T. H. Davies, E. Follana, K. Hornbostel, and G. P. Lepage, Heavy meson masses and decay constants from relativistic heavy quarks in full lattice QCD, *Phys. Rev. D* **86**, 074503 (2012), arXiv:1207.0994 [hep-lat].
- [41] R. J. Dowdall, C. T. H. Davies, T. C. Hammant, and R. R. Horgan, Precise heavy-light meson masses and hyperfine splittings from lattice QCD including charm quarks in the sea, *Phys. Rev. D* **86**, 094510 (2012), arXiv:1207.5149 [hep-lat].
- [42] B. Chakraborty, C. T. H. Davies, B. Galloway, P. Knecht, J. Koponen, G. C. Donald, R. J. Dowdall, G. P. Lepage, and C. McNeile, High-precision quark masses and QCD coupling from $n_f = 4$ lattice QCD, *Phys. Rev. D* **91**, 054508 (2015), arXiv:1408.4169 [hep-lat].

SUPPLEMENTARY INFORMATION

Below we detail the procedure utilized in the extraction of energy levels from the correlation functions. Afterwards, the statistical and systematic uncertainties in the binding energy of \mathcal{D}_{6b} dibaryon determined from these estimates are quantified.

Energy extraction: The Euclidean two-point correlation functions in Eq. (3) at large source-sink separations τ are fitted with single exponentials of the form

$$\langle C(\tau) \rangle = W_0 e^{-E_0 \tau}, \quad (9)$$

using correlated χ^2 and maximum likelihood estimators to extract E_0 and W_0 . In Figure 7 we present such a result showing the projections of posterior probability distributions of the parameters E_0 and W demonstrating the reliability of the fits for the example of \mathcal{D}_{6b} correlation functions in the finest ensemble.

In order to quantify the uncertainties arising from the choice of fitting window (τ_{min}, τ_{max}) , we do the following. First choose a τ_{max} as large as possible with a good signal-to-noise ratio. Then the τ_{min} is varied over a range to determine the stability of E_0 estimate and a τ_{min} value is chosen where a clear plateau is observed. A conservative estimate taking account of an uncertainty on this choice is arrived at using a correlated average over neighboring τ_{min} values in the plateau. In Figure 3 (main

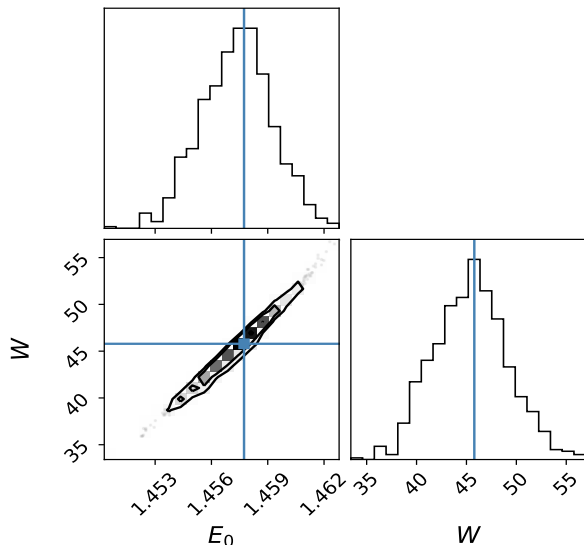


FIG. 7. The multivariate distribution of fitted parameters E_0 and W (bottom left) and their respective univariate distributions (Top left) and (Bottom right).

text) and Figure 8, we present the τ_{min} dependence for all the fits along with the 1σ statistical errors for the chosen fit window (blue bands), and the final estimate considering the uncertainty from the chosen fitting window (magenta bands). In both figures, we present the estimates for the non-interacting two-baryons on the left and for the dibaryons \mathcal{D}_{6b} on the right. These estimates are then utilized to arrive at the energy differences in Eq. (4) and Table I.

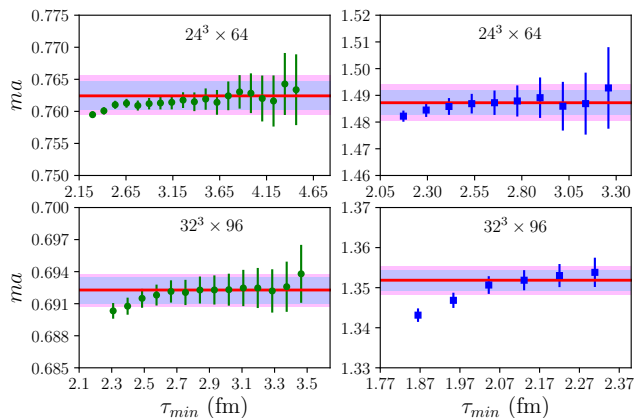


FIG. 8. Fit results for the ground state masses for different fit-windows corresponding to various choices of minimum time (τ_{min}).

It should be mentioned here that we do not use the ratio-method for extracting the energy difference. As is evident from the Figure 2, due to a large energy difference, the ground states of the single baryon (Ω_{bbb}) and

the dibaryon (\mathcal{D}_{6b}) reach to their respective saturation at two very different times. Taking ratio of these correlators at a given time, in this case, may lead to a precise but inaccurate result.

Error Analysis: The main source of error in a lattice QCD calculation involving multiple hadrons is from the rapid decrease of the signal-to-noise ratio in the correlation functions [38]. In heavy hadrons, this is somewhat mitigated due to the presence of heavy quarks. In this calculation since all the valence quarks are of bottom flavor and no chiral dynamics is involved, it is expected to have a relatively better signal-to-noise ratio than that of other dibaryons. Nevertheless, different systematics need to be addressed, particularly discretization errors, to arrive at a reliable estimate for the binding energy of the \mathcal{D}_{6b} dibaryon. We discuss various relevant systematics involved in our calculation below.

Excited states and statistical errors: Coulomb gauge fixed wall sources are utilized for the quark fields, which gives an early ground state saturation with highly suppressed excited states contamination. We also consider fitting windows that are above 2 fm. For a compact state like \mathcal{D}_{6b} , this is sufficiently large to make sure of the ground state signal saturation. We also average the correlation functions over multiple source time-slices to improve the statistical uncertainties. In addition to this, we follow the procedure outlined in the previous section to include fit-window uncertainties, and arrive at the final energies and energy differences presented in the main text. We find these uncertainties amount to 9-17% on finer to coarser ensembles that we used.

Continuum extrapolation: We employ a set of lattice QCD ensembles in which gauge fields are Symanzik-improved at $\mathcal{O}(\alpha_s a^2)$ and include the effect of u , d , s and c quark vacuum polarization generated with the highly improved staggered quark action [21]. Quark propagators are generated with NRQCD action with improvement coefficients up to $\mathcal{O}(\alpha_s v^4)$. The lattice spacing dependence of the energy differences in Table I could be nontrivial. Similar to the approach made in Ref. [10], we account for this by parameterizing $kcot\delta_0$, that enter the scattering analysis in Eq. (5), with different forms and perform fits with different sets of energy levels determined from the simulation. Choosing the linear parameterization $kcot\delta_0 = -1/a_0^{[0]} - a/a_0^{[1]}$ that best describes the entire data, we find the total uncertainties arising from statistics, fitting window and continuum extrapolation to be $\sim 18\%$ of the binding energy from the continuum extrapolation. We find that choosing other forms of continuum extrapolation for the scattering length $-1/a_0$ leads to a change of at most 8 MeV in the binding energy, which we quantify as the uncertainty arising from the discretization error.

Scale setting: Scale settings through r_1 parameter [21] and Wilson-flow were found to be consistent [21] for these

lattice ensembles. Systematics with the scale settings further gets reduced in the estimation of energy differences (Eq. 4), and as in Ref. [11, 20] we find it to be maximum of about 3 MeV.

Quark mass tuning: We tune the bottom quark mass employing the Fermilab method of heavy quarks [26]. Here, we equate the lattice extracted spin average $1S$ bottomonia *kinetic mass*, $\frac{1}{4}[3M_\Upsilon + M_{\eta_b}]_{kin}$, with its physical value. We perform this tuning corresponding to the central value of the chosen scale and also at its error values. We calculate $E_{\mathcal{D}_{6b}}$ for each of the tuned masses and include the variation as the estimation of error due to quark mass tuning. We find it to be less than 2 MeV.

With the above mentioned lattice-set up we find the hyperfine splitting in $1S$ bottomonia, a benchmark observable for the evaluation of the goodness of lattice calculations with bottom quarks, is quite consistent with its experimental value, as demonstrated in Figure 9. The continuum value (green star) is obtained taking the average of estimates from all ensembles and the error (green band) is estimated as a weighted average with respect to the lattice spacings. Continuum extrapolation with the linear as well as and quadratic forms in lattice spacing are also shown by the orange and blue stars respectively with the same color bands for their $1-\sigma$ errors. Together with possible other systematics, that we are discussing here, we estimate its value to be $62.6(3)(5)$ MeV.

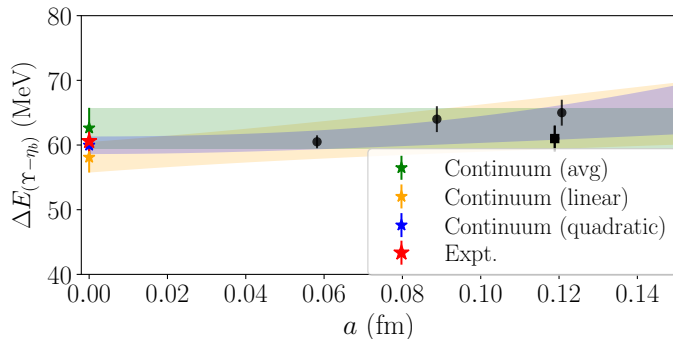


FIG. 9. Hyperfine-splitting of the $1S$ bottomonia.

Electromagnetism: The dibaryon investigated here has two units of electric charge and can have substantial Coulomb repulsion. We model each $\Omega_{bb\bar{b}}$ as a compact particle, but with a finite charge radius (r_d), with an exponential charge distribution as in Ref. [12]. This leads to the Coulomb potential as in Eq. (6) of Ref. [12], but with a total electric charge of -2 . We then solve the non-relativistic Schrödinger equation with this potential by varying r_d in between $0.01 - 0.5$ fm, covering the *rms* radius of the ground state wave-function of the parameterized strong potential. We find the change in binding energy to be $5-10$ MeV within this range of r_d . For heavy baryons, the possible systematics due to electromagnetic corrections was found to be 3 MeV [39]. Keeping that in mind as the source of other electromagnetic effects beside the Coulomb repulsion, we take a conservative estimate of 8 MeV corrections for the binding energy (by adding the average of Coulomb repulsion with the above mentioned 3 MeV in quadrature).

No chiral extrapolation is necessary for \mathcal{D}_{6b} . For heavier dibaryons the unphysical sea quark mass effects are expected to be within a percent level [40–42], and particularly for \mathcal{D}_{6b} , it would be negligibly small. In Table II we summarize the error-budget estimate where above mentioned systematics are added in quadrature.

Source	Error (MeV)
Statistical + Fit-window + Continuum extrapolation	$\begin{pmatrix} +16 \\ -12 \end{pmatrix}$
Discretization	8
Scale setting	3
m_b tuning	2
Electromagnetism	8
Total systematics	12

TABLE II. Error budget in the calculation of the binding energy $\Delta E_{\mathcal{D}_{6b}}$.